One-Dimensional Self-Assembly of Polyaromatic Compounds Revealed by Molecular Dynamics Simulations

ARTICLE *in* THE JOURNAL OF PHYSICAL CHEMISTRY B · OCTOBER 2014

Impact Factor: 3.3 · DOI: 10.1021/jp506381z · Source: PubMed

2 AUTHORS:

Cuiying Jian
University of Alberta
5 PUBLICATIONS **24** CITATIONS
SEE PROFILE

Tian Tang
University of Alberta
62 PUBLICATIONS **778** CITATIONS
SEE PROFILE

THE JOURNAL OF PHYSICAL CHEMISTRY B

Article

pubs.acs.org/JPCB

One-Dimensional Self-Assembly of Polyaromatic Compounds Revealed by Molecular Dynamics Simulations

Cuiying Jian and Tian Tang*

Department of Mechanical Engineering, University of Alberta, Edmonton, Alberta T6G 2G8, Canada

Supporting Information

ABSTRACT: A series of molecular dynamics simulations were performed on the self-assembly of polyaromatic (PA) compounds in *n*-heptane. These compounds possess the same PA core but systematically varied side-chain lengths. Regardless of the side-chain lengths, the simulations revealed the formation of one-dimensional (1D) self-assemblies resulting mainly from parallel stacked PA cores. The length over which the parallel stacking persists was found to be 3−5.6 nm. The 1D self-assembly was not observed for the same PA compounds in water or toluene, suggesting the importance of solvent properties in its formation. In particular, *n*-heptane can prevent the side chains from interfering with PA core stacking while having limited attraction with the cores, which facilitates the 1D self-assembling. These findings, revealed at the molecular level, provide insights into controlling the self-assembling process in the design of optical and electronic nanodevices.

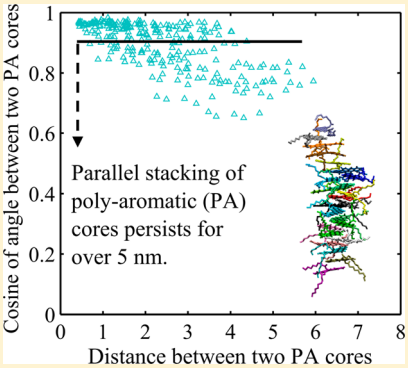

1. INTRODUCTION

Polyaromatic (PA) compounds are a broadly defined class of condensed homocyclic or heterocyclic aromatic rings.[1] They have π-conjugated molecular structures and are widely found in a variety of environmental samples including water and soil,[2] as well as in novel functional materials.[3] Industrial PA compounds such as asphaltenes in oil sands usually consist of fused heterocyclic aromatic rings with substituted side chains and heteroatoms, for example, oxygen, nitrogen, and sulfur.[4] Under certain conditions, PA compounds have been observed to self-associate and form aggregates. The aggregated structures have wide applications such as being used in light-harvesting arrays,[5,6] organic thin film transistors,[7,8] liquid crystals,[9,10] laser dyes,[11] and organic solar cells.[12] On the other hand, the highly stable aggregates can also have serious adverse effects on a number of industrial processes, such as upgrading, refinery and recovery, and water treatment in oil sand production.[13−15] Through experimental and theoretical methods, self-association of many natural and synthetic PA compounds have been studied, examples including perylene tetracarboxylic diimide (PTCDI) derivatives,[16] hexabenzocoronene (HBC) derivatives,[16] and pyrene derivatives.[17] For instance, it was revealed,[18−20] by scanning electron microscopy (SEM), transmission electron microscopy (TEM), and atomic force microscopy (AFM), that vesicles, micelles, or nanocoils could be obtained from self-association of PTCDI or HBC derivatives. Using nuclear magnetic resonance (NMR) spectroscopy, steady-state fluorescence spectroscopy, vapor pressure osmometry (VPO), single-crystal X-ray diffraction, and thermogravimetric analysis, 4,4′-bis(2-pyren-1-yl-ethyl)-[2,2′] bipyridinyl (PBP) was shown to self-associate in chloroform when the PBP concentration exceeded 6×10^{-6} M and form dimers in toluene when its concentration was beyond 1.5×10^{-5} M.[21] Recently, a series of computational studies at atomic level revealed stacked parallel PA cores for PA molecules in water and organic solvents.[22−27]

One particularly interesting category of aggregates formed by PA compounds is a one-dimensional (1D) rod-like self-assembly. Such a structure was proposed[28,29] to be formed by face-to-face $\pi-\pi$ stacking of PA cores (see an ideal representation in Figure 1) and has promising applications in optical and electronic nanodevices.[28,29] A large amount of

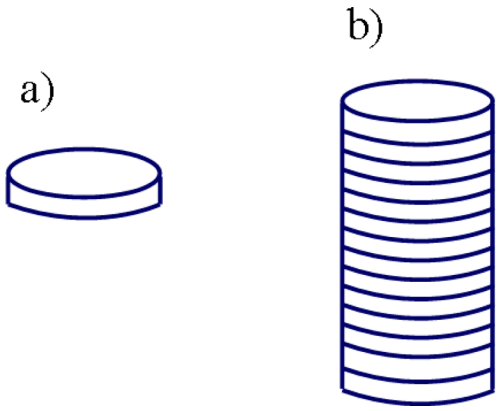

Figure 1. Schematic representation of (a) a single PA core and (b) a 1D structure formed by perfect face-to-face stacking of PA cores. Note that offset stacking can also be found in such a 1D structure but is not shown here.

Received: June 26, 2014
Revised: October 10, 2014
Published: October 10, 2014

experimental work has focused on investigating suitable PA compounds that can efficiently self-assemble into 1D structures. For instance, trialkylphenyl-functionalized PTCDI in methylcyclohexane, at a concentration of 5.0×10^{-3} M, was revealed[18] by VPO measurements to form extended stacks of nine, seven, and six molecules at 40, 50 and 60 °C respectively, which agreed well with the sizes found[18,19] by UV/vis spectroscopy. Through a surface X-ray diffraction study, it was shown that[30] highly ordered hexa(3,7-dimethyl-octanyl)hexa-peri-hexabenzocoronene (HBC-C8,2) films of uniaxially aligned PA cores could be fabricated by crystallization from cyclohexanone solution onto friction-transferred poly(tetrafluoroethylene) layers.

The existence of such a 1D structure appears to strongly depend on the molecular structure of PA compounds. Investigated by AFM, the morphology of aggregates formed by two peptide-functionalized PTCDIs in aqueous buffer was revealed[31] to change from chiral nanofibers to spherical shapes, depending on the nature of peptide used in the molecule. Dodecyloxy- and thiododecyl-substituted PTCDIs were shown by TEM, SEM, and AFM to exhibit different aggregation behaviors in methanol; nanowires were observed for PTCDI compounds with two dodecyloxy groups, while spherical particles were found for PTCDI compounds with two thiododecyl groups.[32] Within the 1D stacked structures, it has been revealed[33] by X-ray scattering that substituents of HBCs, such as alkyl, phenyl alkyl, carboxyl, cyano, or bromo, can tune the packing organization of PA cores.

The property of the solvent is another factor that influences the structure of the aggregates. Alkyl-substituted PTCDIs, for example, PTCDI-C_8, formed a homogeneous solution in chloroform (a "good" solvent) at the concentration of 1 g/L, while 1D microstructures were observed by SEM and TEM after an equal amount of methanol (a "poor" solvent) was added to the above solution.[34] In our previous work,[25,27] molecular dynamics (MD) simulations performed on violnthrone-78 (VO-78)-based PA models revealed distinct aggregated structures in water and toluene. In water, while some stacking between PA cores was observed, most PA molecules were simply entangled together without apparent order, and the final geometry formed by PA cores was close to a 3D sphere. In toluene, however, the largest stable aggregate consisted of less than 11 molecules with their PA cores parallel stacked, thus the interior core region resembling the geometry of a short cylinder. Such different geometries are caused by different aggregation mechanisms in the two solvents; in water, besides $\pi-\pi$ interaction between the PA cores, additional hydrophobic association exists among the aliphatic side chains to minimize their contact with water, leading to sphere-like aggregates, while in toluene, hydrophobic association is absent and $\pi-\pi$ interaction dominates, resulting in aggregates consisting solely of parallel stacked PA molecules.

In addition, even for a given solvent and PA compounds with a certain molecular structure, the geometry of the aggregates can be affected by the concentration of the solution. For instance, as the concentration of propyl-substituted PICDIs in water increases from 1×10^{-7} to 1×10^{-4} M, the UV/vis spectra indicated a more ordered molecular arrangement inside the aggregate.[35] Characterized by SEM, self-assemblies formed by T-shaped bisphenazine in deuterated chloroform with different concentrations showed morphological transformation from straight strands to nanofiber bundles with substantial coiling and further to flat nanofibers with less bundling and coiling.[36]

n-Heptane, like water, is also considered a poor solvent for PA compounds in petroleum engineering.[37,38] However, *n*-heptane molecules are apolar compared with water, and it has been suggested[39] in the literature that *n*-hexane (of similar chemical structure as *n*-heptane) can enhance the $\pi-\pi$ interaction between VO-based PA molecules. Hence, aggregates of these molecules may exhibit different geometries in *n*-heptane compared with that in water or toluene. In this work, we report MD simulation results for the self-assembly of VO-78-based model compounds in *n*-heptane. The molecular models employed here, which have great potential use in organic photovoltaic devices, near-infrared (NIR) OLEDs, and photodetectors,[39,40] possess the common features of PA compounds, and therefore, the results may be applied to a broader class. Our simulation reveals that in *n*-heptane, the PA molecules self-assemble into 1D rod-like structures with long-range stacking order, which was not observed in our previous studies where water and toluene were the solvents,[25,27] suggesting that the aggregation mechanism in *n*-heptane may be very different from that in water or toluene. The remainder of the paper is organized as follows: the molecular models and computational methods used in this study are introduced in section 2; in sections 3 and 4, simulation results allow us to examine and discuss the self-assembled structures in detail; final conclusion is given in section 5.

2. METHOD

2.1. Molecular Models. Chemical structures of the four PA molecular models employed in this work are shown in Figure 2.

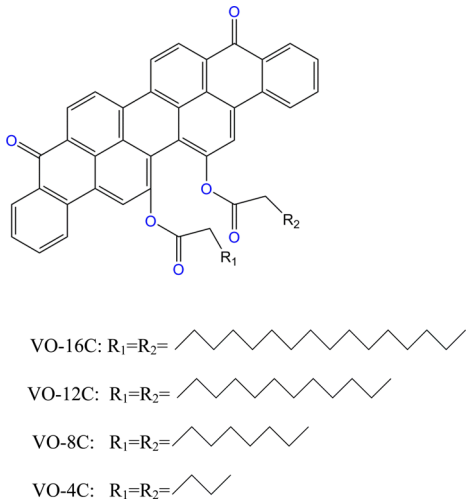

Figure 2. Chemical structures of the PA molecular models employed in this work.

These models were developed based on VO-78, which consists of nine fused aromatic rings, two aliphatic side chains, and six oxygen atoms as heteroatoms. The hydrogen-saturated parts of the side chains (R_1 and R_2 in Figure 2) are completely uncharged, while the PA core region has certain polarity. The original VO-78 model has 16 interconnected aliphatic hydrocarbons on each of R_1 and R_2 and will be referred to as VO-16C. Because it is typically believed that[41] the $\pi-\pi$ interaction between PA cores promotes aggregation while the side chains interfere with it, three additional models were introduced by

dx.doi.org/10.1021/jp506381z | J. Phys. Chem. B 2014, 118, 12772−12780

varying the length of the side chains relative to the PA core. The structure of VO-16C was constructed by Chem3D ultra 10.0, and structures of the other three models were obtained by manually removing a certain number of aliphatic hydrocarbons from each side chain of VO-16C. For instance, VO-12C in Figure 2 was developed by removing four aliphatic hydrocarbons from each chain. The aliphatic/aromatic ratio, defined as the ratio between the total number of interconnected aliphatic hydrocarbons on the side chains (R_1 and R_2) and the number of aromatic carbons in the PA core, are, respectively, 0.94, 0.71, 0.47, and 0.24 for VO-16C, VO-12C, VO-8C, and VO-4C in Figure 2. *n*-Heptane, the solvent used in this work, is a linear chain alkane.

The topology for each PA model was validated in our previous work[25] and directly adopted here. The functional groups, atom types, and their partial charges are given in the Supporting Information (section S1). The topology for *n*-heptane was generated based on dipalmitoylphosphatidylcholine (DPPC) in the GROMOS96 force field parameter set 53A6[42] through the pdb 2gmx routine in GROMACS.[43−46] The topology validation for *n*-heptane is available in the Supporting Information (section S2).

2.2. Simulation Details. Four systems were simulated, named, VO-16C, VO-12C, VO-8C, and VO-4C, each containing a single type of molecular model described in section 2.1. In constructing the initial configuration of each system, an ordered 2 × 3 × 4 array of 24 PA molecules was packed into a cubic box of dimension 12 × 12 × 12 nm^3, with the PA cores parallel with one another. The spacing between the mass centers of two neighboring PA molecules is, respectively, 5.2, 3, and 2.6 nm in the three directions, which is much larger than the characteristic length for $\pi-\pi$ stacking distance (~0.45 nm). Therefore, although the PA cores are arranged in a parallel manner in the initial configuration, it should not lead to unrealistic trapping of the molecules in parallel stacked configurations. This was proven[25] in our earlier simulations for the same PA compounds in water, where initially parallel PA molecules form disordered sphere-like aggregates at the end of the simulation. Following this, the simulation boxes were randomly filled with *n*-heptane molecules, resulting in a solute mass concentration of ~3.8, 3.4, 3.0, and 2.6%, respectively, for systems VO-16C, VO-12C, VO-8C, and VO-4C. Inside each simulation box, the number of *n*-heptane molecules is ~6100, and its initial bulk density is ~650 g/L, close to the literature value[47] of 679 g/L.

All simulations were performed using the MD package GROMACS (version 4.0.7) with periodic boundary conditions applied. During each simulation, static structure optimization was first performed, followed by 1 ns position-restrained simulations at 300 K and 1 bar, where the harmonic potential was applied on the non-hydrogen atoms of the solutes with a spring constant of 1000 kJ/(mol·nm^2) while the solvent molecules were allowed to relax around the solutes. The restraint was then removed, and full dynamics simulation was performed in the *NPT* ensemble for 180 ns. The pressure and temperature were controlled by a Parrinello−Rahman barostat[48] and a velocity rescaling thermostat,[49] respectively; the latter is based on correctly producing the probability distribution of kinetic energy under constant temperature and differs from the isokinetic scheme[50] of maintaining constant temperature. For all dynamics simulations, the integration time step was 2 fs; intramolecular bonds were constrained by the LINCS algorithm;[51] full electrostatics was treated by the particle mesh Ewald method;[52] and van der Waals interactions were evaluated by the twin range cutoff approach.[53]

2.3. Data Analysis. Appropriate postprocessing programs available in GROMACS were used for trajectory analysis, and VMD[54] was used for visualization. Unless otherwise specified, all analysis was based on the average over the last 20 ns of the simulation. Demonstration for the achievement of dynamic equilibrium is available in the Supporting Information, section S3.

A quantity useful for describing the geometry of a structure is the radius of gyration. Two types of radius of gyration have been employed in this work, the radius of gyration about the center of mass and the principal radii of gyration. The radius of gyration R_g about the center of mass is calculated by[55]

$$R_g = \left(\frac{\sum_i m_i r_i^2}{\sum_i m_i} \right)^{0.5} \quad (1)$$

where m_i and r_i are, respectively, the mass and distance from the center of mass for atom i, $\sum_i m_i$ is the total atomic mass, and $\sum_i m_i r_i^2$ is the mass moment of inertia. Passing through the center of mass, three principal axes can be found and will be denoted by x, y, and z. Radii of gyration about these principal axes are calculated by[55]

$$R_x = \left(\frac{\sum_i m_i (y_i^2 + z_i^2)}{\sum_i m_i} \right)^{0.5} \quad (2)$$

$$R_y = \left(\frac{\sum_i m_i (x_i^2 + z_i^2)}{\sum_i m_i} \right)^{0.5} \quad (3)$$

$$R_z = \left(\frac{\sum_i m_i (x_i^2 + y_i^2)}{\sum_i m_i} \right)^{0.5} \quad (4)$$

where (x_i, y_i, z_i) are the coordinates for atom i and the summations are over all atoms in the molecular structure of interest. After $\{R_x, R_y, R_z\}$ are computed, we further denote R_0 as the minimum of $\{R_x, R_y, R_z\}$, R_2 as the maximum of $\{R_x, R_y, R_z\}$, and R_1 as the intermediate value. For a 1D structure, the length scale in one direction will be much larger than that in the other two. Hence, $R_0 \ll R_1 \approx R_2$. In contrast, for a sphere-like structure, because the three dimensions are approximately equal, $R_0 \approx R_1 \approx R_2$. For structures that resemble short cylinders, $R_0 < R_1 \approx R_2$. Therefore, the relative magnitude of R_0, R_1, and R_2 is a good indicator for the dimension characteristics of the structure. Furthermore, these geometry descriptions can also be applied to a subset of the atoms in the structure. In this case, the summations in eqs 2, 3, and 4 should be performed over atoms in the subset.

3. RESULTS

Figure 3 shows the snapshots of the largest stable self-assemblies in the four systems, that is, the ones that do not dissociate at the equilibrium stage of the simulations. All self-assemblies shown are formed by the molecules contained in the primitive simulation cells. In systems VO-4C, VO-8C, and VO-12C, the largest stable self-assembly involves all 24 molecules, whereas in system VO-16C, the largest stable self-assembly contains 16 molecules. It can be clearly seen from Figure 3 that irrespective of the aliphatic/aromatic ratios, the dominant structures are formed by the parallel stacking of multiple PA

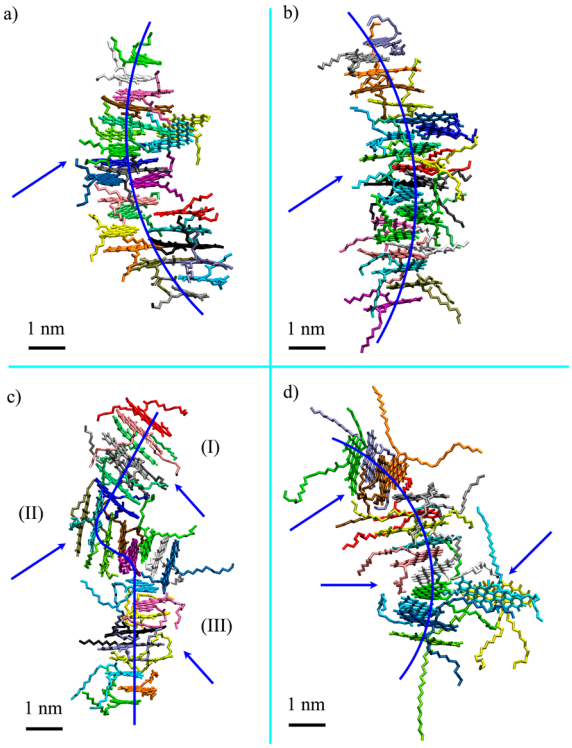

Figure 3. Snapshots of the largest stable self-assemblies formed at the equilibrium stage of the simulations in systems (a) VO-4C, (b) VO-8C, (c) VO-12C, and (d) VO-16C. In the first 3 systems, the largest stable self-assembly involves all 24 molecules in the simulation box. In system VO-16C, besides the largest stable self-assembly, there are two additional small aggregates (not shown), each involving four molecules. (I), (II), and (III) in (c) show the three stacks of parallel PA cores in the largest stable self-assembly formed in system VO-12C.

cores, indicated by the blue arrows in Figure 3. For instance, there are three stacks of parallel-aligned PA cores in the largest stable self-assembly formed in system VO-12C, labeled as (I), (II), and (III), respectively. More interestingly, there exists a clear axis in each self-assembly, depicted as blue curves in Figure 3, along which the stacking of the PA cores is propagated. This suggests the formation of 1D rod-like structures with a certain degree of bending flexibility. These structures found from our simulations show great similarities to SEM, TEM, AFM, and fluorescence microscopy results[56,57] on organic semiconductors, where large PA cores with linear aliphatic side-chain substitutions were observed to form a 1D nanobelt. In addition, unlike the ideal parallel stacking shown in Figure 1b, the self-assemblies obtained in our simulations all involve molecular tilting, slipping, and twisting along the stacking axis. The formation of a 1D ideal parallel stacking structure requires significant reduction in entropy, which can in turn increase the free energy of the system although such stacking also tends to reduce the free energy by decreasing enthalpy. Therefore, it is entirely possible to have some titling, slipping, and twisting, as resulted from the enthalpy/entropy competition.

To quantitatively confirm and describe the 1D self-assembly, we first plotted, in Figure 4, the radial distribution functions (RDFs) for the center of geometry (COG) distances r (nm) between any two PA cores. For each of the four systems, there exist multiple peaks in the RDFs, the first four located at approximately r = 0.45, 0.75, 1.1, and 1.5 nm, respectively. At

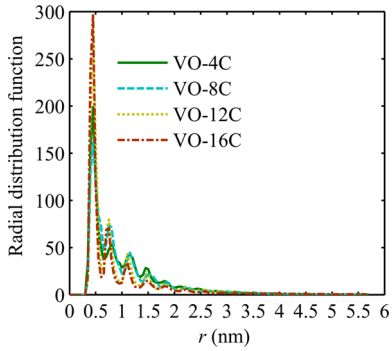

Figure 4. RDFs for the COG separation distance r (nm) between two PA cores. Each peak in the RDFs corresponds to high density of PA cores at this location. The first four peaks for the four systems are, respectively, located at 0.45, 0.80, 1.15, and 1.45 nm for VO-4C, 0.45, 0.75, 1.15, and 1.50 nm for VO-8C, 0.45, 0.75, 1.10, and 1.50 nm for VO-12C, and 0.45, 0.75, 1.10, and 1.50 nm for VO-16C.

these COG separations, to probe the relative orientation of PA cores, we calculated the cosine of angle σ ($\cos\sigma$) between any two PA core planes. If two PA core planes are close to being parallel, then it is expected that $\cos\sigma$ will be near 1. Figure 5

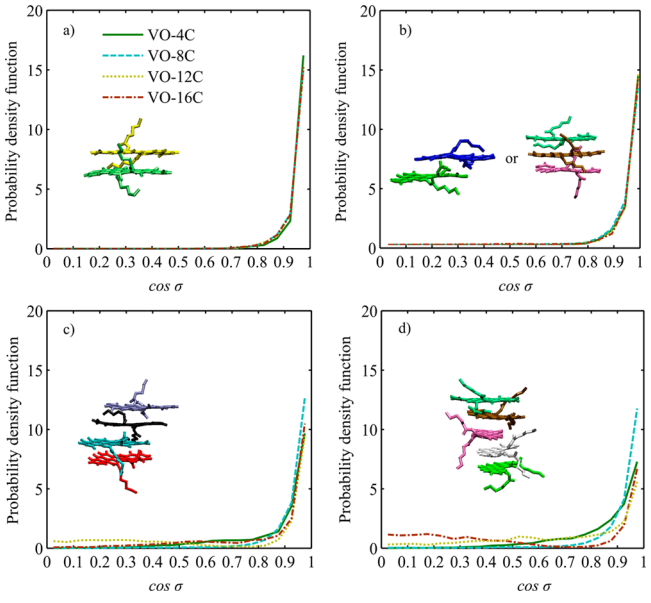

Figure 5. PDFs for $\cos\sigma$ at COG separation distances of (a) 0.45, (b) 0.75, (c) 1.1, and (d) 1.5 nm. The peak at $\cos\sigma \approx 1$ in each subfigure corresponds to a parallel stacking configuration that is shown as the inset.

shows the probability density functions (PDFs) for $\cos\sigma$ at the first four RDF peaks. Clearly, in each subfigure, the PDFs have their sole and pronounced peaks at $\cos\sigma \approx 1$, confirming the parallel stacking configuration of PA cores at these COG separations. The four curves in the subfigures are only distinguishable for r > 1 nm (Figure 5c and d), and even at r > 1 nm, they only differ quantitatively, suggesting similar parallel stacking configurations regardless of the aliphatic/aromatic ratios. The parallel stacking at 0.45 nm (Figure 5a) corresponds to π–π stacked PA cores where the COG of one core is directly on top of the other (inset in Figure 5a). The parallel stacking at 0.75 nm (Figure 5b) can correspond to two different configurations (insets in Figure 5b); in the first one,

dx.doi.org/10.1021/jp506381z | J. Phys. Chem. B 2014, 118, 12772−12780

the PA core is still on top of the other but is shifted laterally so that the line connecting the two COGs is not perpendicular to the cores (left inset in Figure 5b); the second configuration results from parallel alignment of two PA cores that have a third PA core sandwiched between them (right inset in Figure 5b). The PDF peaks at r = 1.1 and 1.5 nm (Figure 5c and d) correspond to parallel alignment of two PA cores when there are two or three other PA cores sandwiched in between (insets in Figure 5c and d, respectively). Therefore, these plots confirm the parallel stacking of multiple PA cores visually observed from Figure 3.

Although the peaks in Figure 4 become considerably smaller after 1.5 nm, the parallel stacking of PA cores persists for a distance much longer than 1.5 nm. Figure 6 shows cos σ versus

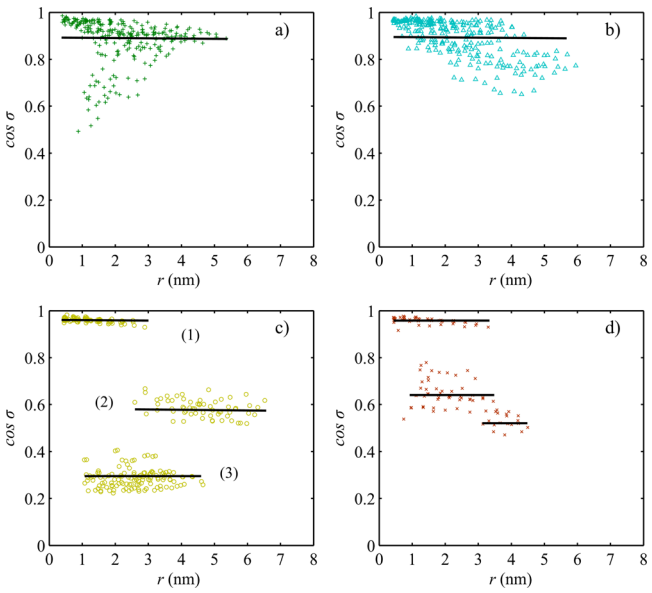

Figure 6. cos σ verus COG distance r for the largest stable assemblies in systems (a) VO-4C, (b) VO-8C, (c) VO-12C, and (d) VO-16C. A horizontal segment is drawn to show the average cos σ value for each group of data, and the rightmost point of the segment for the cos $\sigma \approx$ 1 group in each subfigure represents the persistence length of parallel stacking in *n*-heptane. The long persistence length for PA compounds in *n*-heptane is consistent with previous observation of a 1D rod-like structure shown in Figure 3

COG distance r for the largest stable self-assemblies formed in the four systems (snapshots shown in Figure 3). Each plot was generated by calculating the COG distance and cos σ between any pair of PA cores in the largest stable self-assembly, averaged over the last 20 ns of the simulation. In each of the three systems VO-4C, VO-8C, and VO-12C, the largest stable self-assembly consists of all 24 molecules; hence there are in total $c_{24}^2 = (24 \times 23)/2 = 276$ pairs of PA cores and 276 data points. There are 16 molecules in the largest stable self-assembly formed in system VO-16C, resulting in $c_{16}^2 = (16 \times 15)/2 = 120$ data points in Figure 6d. Let us first consider Figure 6a, for system VO-4C, where most data points are distributed around cos σ = 0.88. This is consistent with the nearly parallel stacking of all 24 PA cores shown in Figure 3a. A horizontal segment is drawn in Figure 6a to show the average cos σ value (0.88). The start and end points of the segment are determined by first identifying data that differ from the average (0.88) by 10% or less. Within this group of data, the smallest r value was used as the leftmost point of the segment, and the largest r value was used as the rightmost point. The leftmost point is in fact located at r = 0.45 nm, corresponding to the direct parallel stacking of two neighboring PA cores, as shown in Figure 5a. The rightmost point of the segment is located at r = 5.5 nm, which corresponds to the COG distance between the lowest and highest PA cores shown in Figure 3a. This implies that the parallel stacking of PA cores persists for at least (given that only 24 molecules were simulated) 5.5 nm along the axis of the self-assembly. This length will be referred to as the persistence length of parallel stacking for the self-assembly, which quantifies the range of parallel stacking.

Similar segments are drawn in Figure 6b–d to show the location of data. Figure 6b exhibits great similarity to Figure 6a, and the persistence length for VO-8C is 5.6 nm. Unlike in Figure 6a and b, data in Figure 6c, for system VO-12C, can be separated into three different groups, (1) near cos σ = 1, (2) near cos σ = 0.6, and (3) near cos σ = 0.3. Thus, three segments are drawn to show the average cos σ value and range of r for each group of data. Consistently, the self-assembly in Figure 3c also contains three stacks of parallel PA cores that are labeled as (I), (II), and (III), respectively. Data group (1) corresponds to parallel stacking within each stack (I), (II), or (III). Data in group (2) correspond to PA core pairs with one from stack (I), and the other are from stack (III). The leftmost point (~2.4 nm) is the COG distance between the two closest molecules from stacks (I) and (III), and the rightmost point (~6.6 nm) is the COG distance between the two furthest molecules from the two stacks. The average cos σ value for group (2), 0.59, implies that the angle between the two stacks is ~54°. Data in group (3) are obtained from PA core pairs with one from stack (I) and the other from stack (II) or with one from stack (II) and the other from stack (III). The average cos σ value is 0.29, indicating that the angle between neighboring stacks is ~73°. Because data group (1) represents parallel alignment within each stack, its range of r is the persistence length for VO-12C, evaluated to be 3 nm. Self-assembly in VO-16C is similar to that in VO-12C, and the data in Figure 6d can also be separated into three groups. The persistence length, calculated based on data near cos σ = 1, is about 3.4 nm. Comparing data in Figure 6, it can be learned that as the length of the side chains increases, the persistence length shows a decreasing trend. Nevertheless, the shortest persistence length found in our simulations is still ~3 nm, which, considering that the COG separation distance between directly parallel stacked PA cores is about 0.45 nm, corresponds to approximately eight parallel-aligned PA cores.

The existence of 1D rod-like self-assembly strongly depends on the type of solvent. The same PA molecules were previously simulated in water and in toluene;[25,27] however, the formation of 1D rods is only observed in *n*-heptane. Figure 7 shows the cos σ versus COG separation distance for the largest stable aggregates in water and in toluene. It can be clearly seen that data points in water are randomly distributed over the range of cos σ = 0.2–1, demonstrating the random orientation of PA cores with respect to one another inside the largest stable aggregates. That is, the PA compounds do not self-assemble into an ordered structure in water. For PA compounds in toluene, most of the data points are distributed between cos σ = 0.8 and 1, corresponding to the previous observation[27] that aggregates formed in toluene mainly consisted of nearly parallel stacked PA cores. However, compared with that in *n*-heptane, the persistence length of parallel stacking in toluene is much smaller, ~2.2 nm for VO-4C and ~2 nm for VO-8C, VO-12C,

dx.doi.org/10.1021/jp506381z | J. Phys. Chem. B 2014, 118, 12772–12780

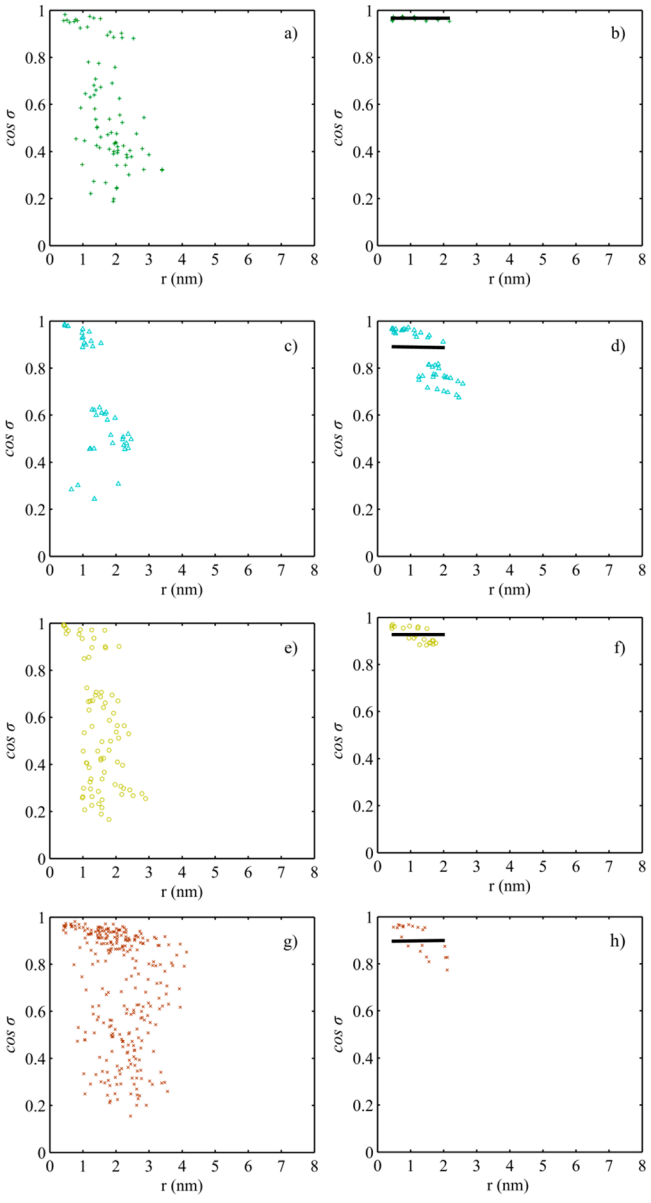

Figure 7. cos σ versus COG separation distance r for the largest stable aggregates in water (left panel) and toluene (right panel) formed by (a,b) VO-4C, (c,d) VO-8C, (e,f) VO-12C, and (g,h) VO-16C. The random distribution of the data points in water confirms the disordered orientation of PA cores inside the aggregate, and the short persistence lengths for PA compounds in toluene verify that the number of PA cores consecutively forming parallel stacking is small.

and VO-16C. This suggests that[27] the largest number of PA cores that can consecutively form parallel stacking in toluene is approximately six in system VO-4C and five in systems VO-8C, VO-12C, and VO-16C.

The lack of stacking order in water and the lack of long-range order in toluene lead to very different geometries formed by the PA cores in these two solvents compared with those in *n*-heptane. Figure 8 shows the three principal radii of gyration (from smallest to largest: R_0, R_1 and R_2) for the PA core regions of the largest stable aggregates in different solvents. It can be clearly seen that for each system in *n*-heptane, R_0, R_1, and R_2 are of the following order: $R_0 \ll R_1 \approx R_2$. In fact, R_2/R_0 are respectively 2.05, 2.44, 2.61, and 2.33 for VO-4C, VO-8C, VO-12C, and VO-16C, which is the characteristic of the 1D rod-like

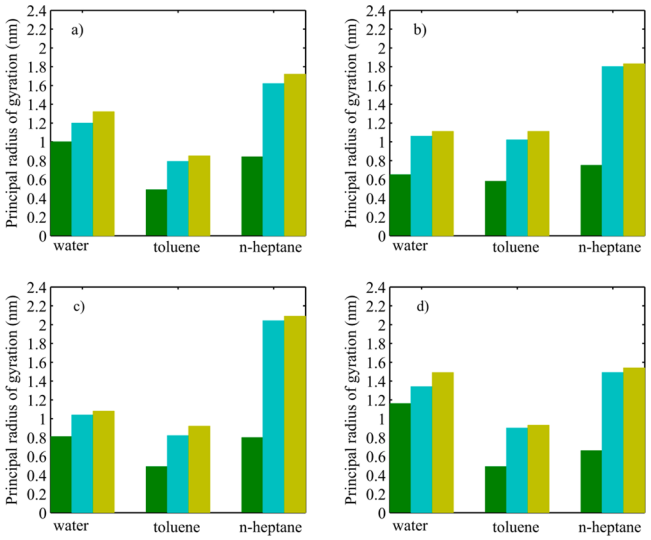

Figure 8. Principal radii of gyration for the PA core regions of the largest stable aggregates in (a) VO-4C, (b) VO-8C, (c) VO-12C, and (d) VO-16C. Each subfigure contains three groups of data, one for a specific solvent (water, toluene, or *n*-heptane). For each group of data, from left to right, R_0, R_1, and R_2.

structures observed in Figures 3 and 6. For toluene, R_1 and R_2 are again close, but unlike in *n*-heptane, they are not significantly larger than R_0 (R_2/R_0 = 1.73, 1.91, 1.88, and 1.90, respectively, for VO-4C, VO-8C, VO-12C, and VO-16C), confirming that the stacked PA cores in toluene resemble short cylinders.[27] As for water, R_0, R_1, and R_2 are relatively close for VO-4C, VO-12C, and VO-16C (R_2/R_0 = 1.32, 1.33, and 1.28, respectively), corresponding to sphere-like aggregates.[25] For VO-8C in water, although R_2/R_0 = 1.71, it is still smaller compared to those in toluene and *n*-heptane.

4. DISCUSSION

Formation of aggregates' configurations and geometries is facilitated by specific driving forces that greatly depend on the solvent properties.[58] It has been observed in our previous work[25,27] that $\pi-\pi$ interaction between PA cores is of great importance for PA aggregation, which is confirmed by the prevalence of parallel stacking found in *n*-heptane. On the other hand, the very different structures formed by the same PA molecules in different solvents indicate the importance of interactions between solvent and solute. First, longer side chains have been suggested[25] to provide larger interference with $\pi-\pi$ stacking of PA cores. Although our simulation data in *n*-heptane show an overall decreasing trend in the persistence length as the side-chain length increases, the decrease is not strictly monotonic. For example, the persistence lengths of VO-4C and VO-8C are close to each other, and the persistence length of system VO-12C (~3 nm) is slightly smaller than that of system VO-16C (~3.4 nm). Our simulations further show that for all four systems, the side chains are quite well solvated in *n*-heptane and do not strongly interfere with the stacking of PA cores (see evidence using the radius of gyration; details are in the Supporting Information, section S4). The solvated side chains indicate the existence of attraction between solvent (*n*-heptane) molecules and side chains, which was also observed for PA compounds in toluene.[27] Contrarily, the hydrophobic nature of the side chains results in their entanglement in water, especially for PA compounds with long side chains. These

dx.doi.org/10.1021/jp506381z | J. Phys. Chem. B 2014, 118, 12772−12780

tangled side chains promote and enhance the stability of the aggregation. On the other hand, they prevent the PA cores from forming parallel stacking, leading to disordered, sphere-like aggregates in water.

Second, although similar solvent−side chain attraction was observed for PA compounds in toluene,[27] Figure 7 shows that the persistence length of parallel stacking is much smaller in toluene than that in *n*-heptane. This can be attributed to the additional solvent−PA core attraction that exists in toluene. Indeed, the aromatic cores of toluene can form $\pi-\pi$ interaction with PA molecules and have a certain order around the PA cores.[27] This additional solvent−solute attraction competes with the attraction among solutes and reduces the number of molecules that can simultaneously form parallel stacking. In contrast, the absence of such solvent−PA core attraction in *n*-heptane favors the $\pi-\pi$ interaction among PA cores, leading to a larger number of PA cores stacked together. These observations are consistent with the solubility definition of asphaltenes that these PA compounds represent.

The above comparison allows us to derive the conditions on the solvent under which 1D rod-like self-assembly can be formed from PA compounds. These conditions are expected to be associated with the solvent−solute interactions, and should strongly depend on the molecular structure of the solute. For PA compounds that only possess an aromatic core region, the single role that the solvent has to play is to optimize the parallel $\pi-\pi$ stacking of PA cores. This requires a certain solubility so that the solutes can arrange themselves in a parallel manner along one direction. On the other hand, the solubility cannot be too high to disrupt the long-range parallel stacking. Therefore, the size of the PA core, its polarity, and the polarity of the solvent must be tuned in order to achieve the optimal condition. When PA cores are accompanied by side chains, in order to self-assemble into a 1D rod-like structure, the solvent must play two separate roles. First, the solvent should be able to prevent the side -chains from mutual association and from interfering with parallel stacking of PA cores. This implies that there has to be sufficiently strong attraction between the solvent and the side chains of the PA compounds. Second, the attraction between the solvent and the PA cores should be limited so as not to disrupt the parallel stacking of PA cores. Depending on the nature of the side chains, different solvents can be chosen to achieve the 1D self-assembling of different PA compounds. For instance, for PTCDIs with hydrophilic imide substituents, water is a "good" solvent to interact with side chains, while for PTCDIs with hydrophobic imide substituents, apolar solvent such as methylcyclohexane can efficiently prevent the side-chain association.[18,59] In both solvents, the stacking of PA cores can be maintained,[18,59] and hence, 1D self-assemblies can be obtained for these two PA compounds in different solvents.

Finally, we point out that the simulations in this work were performed for 180 ns, which is longer than any existing MD simulations on PA molecules. Stacked parallel pairs were observed by Headen et al.[26] (mass concentration of PA compounds, ∼7%) and Teklebrhan et al.[24] (mass concentration, ∼3.5%) in their short MD simulations (∼10 or 20 ns), but unlike the dominance of parallel stacking discussed here, tail−tail contact and tail−core contact were also reported as highly possible configurations between adjacent PA molecules. Sedghi et al.[60] conducted 80 ns MD simulations for eight types of PA molecules in *n*-heptane at mass concentrations of ∼7%. For their A03 and A04 molecular models, parallel stacking of multiple PA cores was found, but a 1D rod-like structure was only observed to start forming in the system of A04 molecules. With a short simulation time (∼10 ns), self-assembly with long-range order, such as seen in the present study, was only observed at mass concentrations significantly higher than the ones used in this work (∼3.8, 3.4, 3.0, and 2.6% for systems VO-16C, VO-12C, VO-8C, and VO-4C, respectively). For example, a decamer structure with PA cores facing each other was reported[61] to form in *n*-pentane within 10 ns, where the mass concentration of PA compounds was ∼25%. Similarly, within 10 ns, long-ranged parallel stacking involving as many as 24 PA cores in *n*-heptane was found in the work by Kuznicki et al.,[22] where the mass concentration was ∼38%. These results seem to suggest that at low mass concentrations, a sufficiently long simulation time is required in order to observe the formation of 1D rod-like self-assembly. We indeed performed a series of simulations for the same systems with different simulation times (see Supporting Information section S5), which confirms that simulation time longer than 120 ns is needed to observe the overall aggregation dynamics and the 1D self-assembly. The 1D self-assembling is therefore a process whose rate strongly depends on the concentration.

5. CONCLUSION

In this work, we report MD simulations that revealed the formation of 1D rod-like self-assembly for PA compounds in *n*-heptane. The self-assembly results from parallel stacking of multiple PA cores. The range of stacking, quantified by a persistence length, is 3−5.6 nm, significantly larger than the spacing between two neighboring $\pi-\pi$ stacked PA cores. Increasing the side chain length reduces the persistence length but does not change the 1D nature of the structure. Formation of such a 1D self-assembly is facilitated by two factors, (i) solvent−side chain attraction, which minimizes interference of side chains with core stacking, and (ii) limited solvent−core interaction, which allows for long-ranged stacking. The results reported here help us to gain insight into conditions that favor the formation of 1D self-assembly (e.g., nanorod or nanobelt) that has great potential in optical and electronic nanodevices.

■ ASSOCIATED CONTENT

Supporting Information

Topology details; topology validation for *n*-heptane; demonstration of the achievement of dynamic equilibrium; evidence for the solvation of side chains in *n*-heptane; and discussion of the length of simulation time. This material is available free of charge via the Internet at http://pubs.acs.org.

■ AUTHOR INFORMATION

Corresponding Author

*E-mail: tian.tang@ualberta.ca. Phone: +1-780-492-5467. Fax: +1-780-492-2200.

Notes

The authors declare no competing financial interest.

■ ACKNOWLEDGMENTS

We acknowledge the computing resources and technical support from the Western Canada Research Grid (WestGrid). Financial support for this research from the Natural Sciences and Engineering Research Council (NSERC) of Canada, Canada Foundation for Innovation, Alberta Innovates-Technology Futures (AI-TF) is gratefully acknowledged. C.J.

acknowledges financial support from the University of Alberta Doctoral Recruitment Scholarship, the Jacob H Masliyah Graduate Award in Oil Sands Engineering, and Alberta Innovates Graduate Student Scholarship. The authors acknowledge helpful discussions with Dr. Subir Bhattacharjee.

REFERENCES

(1) Vo-Dinh, T.; Fetzer, J.; Campiglia, A. Monitoring and Characterization of Polyaromatic Compounds in the Environment. *Talanta* **1998**, *47*, 943−969.
(2) Liu, Z.; Laha, S.; Luthy, R. G. Surfactant Solubilization of Polycyclic Aromatic Hydrocarbon Compounds in Soil-Water Suspensions. *Water Sci. Technol.* **1991**, *23*, 475−485.
(3) Hoeben, F. J.; Jonkheijm, P.; Meijer, E.; Schenning, A. P. About Supramolecular Assemblies of π-Conjugated Systems. *Chem. Rev.* **2005**, *105*, 1491−1546.
(4) Groenzin, H.; Mullins, O. C. Asphaltene Molecular Size and Structure. *J. Phys. Chem. A* **1999**, *103*, 11237−11245.
(5) Hippius, C.; Schlosser, F.; Vysotsky, M. O.; Böhmer, V.; Würthner, F. Energy Transfer in Calixarene-Based Cofacial-Positioned Perylene Bisimide Arrays. *J. Am. Chem. Soc.* **2006**, *128*, 3870−3871.
(6) Wong, W. W.; Khoury, T.; Vak, D.; Yan, C.; Jones, D. J.; Crossley, M. J.; Holmes, A. B. A Porphyrin-hexa-peri-hexabenzocoronene-porphyrin Triad: Synthesis, Photophysical Properties and Performance in a Photovoltaic Device. *J. Mater. Chem.* **2010**, *20*, 7005−7014.
(7) Facchetti, A. π-Conjugated Polymers for Organic Electronics and Photovoltaic Cell Applications. *Chem. Mater.* **2010**, *23*, 733−758.
(8) Wong, W. W.; Singh, T. B.; Vak, D.; Pisula, W.; Yan, C.; Feng, X.; Williams, E. L.; Chan, K. L.; Mao, Q.; Jones, D. J. Solution Processable Fluorenyl Hexa-peri-hexabenzocoronenes in Organic Field-Effect Transistors and Solar Cells. *Adv. Funct. Mater.* **2010**, *20*, 927−938.
(9) Mizoshita, N.; Tani, T.; Inagaki, S. Highly Conductive Organosilica Hybrid Films Prepared from a Liquid-Crystal Perylene Bisimide Precursor. *Adv. Funct. Mater.* **2011**, *21*, 3291−3296.
(10) Schmidt-Mende, L.; Fechtenkotter, A.; Mullen, K.; Moons, E.; Friend, R. H.; MacKenzie, J. D. Self-Organized Discotic Liquid Crystals for High-Efficiency Organic Photovoltaics. *Science* **2001**, *293*, 1119−1122.
(11) Díaz-García, M.; Calzado, E.; Villalvilla, J.; Boj, P.; Quintana, J.; Cespedes-Guirao, F.; Fernandez-Lazaro, F.; Sastre-Santos, A. Effect of Structural Modifications in the Laser Properties of Polymer Films Doped with Perylenebisimide Derivatives. *Synth. Met.* **2009**, *159*, 2293−2295.
(12) Choi, H.; Paek, S.; Song, J.; Kim, C.; Cho, N.; Ko, J. Synthesis of Annulated Thiophene Perylene Bisimide Analogues: Their Applications to Bulk Heterojunction Organic Solar Cells. *Chem. Commun.* **2011**, *47*, 5509−5511.
(13) Speight, J. Petroleum Asphaltenes-Part 1: Asphaltenes, Resins and the Structure of Petroleum. *Oil Gas Sci. Technol.* **2004**, *59*, 467−477.
(14) Spiecker, P. M.; Gawrys, K. L.; Trail, C. B.; Kilpatrick, P. K. Effects of Petroleum Resins on Asphaltene Aggregation and Water-in-Oil Emulsion Formation. *Colloids Surf., A* **2003**, *220*, 9−27.
(15) Kilpatrick, P. K. Water-in-Crude Oil Emulsion Stabilization: Review and Unanswered Questions. *Energy Fuels* **2012**, *26*, 4017−4026.
(16) Wang, C.; Dong, H.; Hu, W.; Liu, Y.; Zhu, D. Semiconducting π-Conjugated Systems in Field-Effect Transistors: A Material Odyssey of Organic Electronics. *Chem. Rev.* **2011**, *112*, 2208−2267.
(17) Figueira-Duarte, T. M.; Müllen, K. Pyrene-Based Materials for Organic Electronics. *Chem. Rev.* **2011**, *111*, 7260−7314.
(18) Chen, Z.; Stepanenko, V.; Dehm, V.; Prins, P.; Siebbeles, L. D.; Seibt, J.; Marquetand, P.; Engel, V.; Würthner, F. Photoluminescence and Conductivity of Self-Assembled π−π Stacks of Perylene Bisimide Dyes. *Chem.—Eur. J.* **2007**, *13*, 436−449.
(19) Würthner, F.; Chen, Z.; Dehm, V.; Stepanenko, V. One-Dimensional Luminescent Nanoaggregates of Perylene Bisimides. *Chem. Commun.* **2006**, 1188−1190.
(20) Yamamoto, T.; Fukushima, T.; Yamamoto, Y.; Kosaka, A.; Jin, W.; Ishii, N.; Aida, T. Stabilization of a Kinetically Favored Nanostructure: Surface ROMP of Self-Assembled Conductive Nanocoils from a Norbornene-Appended Hexa-*peri*-hexabenzocoronene. *J. Am. Chem. Soc.* **2006**, *128*, 14337−14340.
(21) Tan, X.; Fenniri, H.; Gray, M. R. Pyrene Derivatives of 2,2′-Bipyridine as Models for Asphaltenes: Synthesis, Characterization, and Supramolecular Organization. *Energy Fuels* **2007**, *22*, 715−720.
(22) Kuznicki, T.; Masliyah, J. H.; Bhattacharjee, S. Molecular Dynamics Study of Model Molecules Resembling Asphaltene-Like Structures in Aqueous Organic Solvent Systems. *Energy Fuels* **2008**, *22*, 2379−2389.
(23) Kuznicki, T.; Masliyah, J. H.; Bhattacharjee, S. Aggregation and Partitioning of Model Asphaltenes at Toluene−Water Interfaces: Molecular Dynamics Simulations. *Energy Fuels* **2009**, *23*, 5027−5035.
(24) Teklebrhan, R. B.; Ge, L.; Bhattacharjee, S.; Xu, Z.; Sjöblom, J. Probing Structure−Nanoaggregation Relations of Polyaromatic Surfactants: A Molecular Dynamics Simulation and Dynamic Light Scattering Study. *J. Phys. Chem. B* **2012**, *116*, 5907−5918.
(25) Jian, C.; Tang, T.; Bhattacharjee, S. Probing the Effect of Side-Chain Length on the Aggregation of a Model Asphaltene Using Molecular Dynamics Simulations. *Energy Fuels* **2013**, *27*, 2057−2067.
(26) Headen, T. F.; Boek, E. S.; Skipper, N. T. Evidence for Asphaltene Nanoaggregation in Toluene and Heptane from Molecular Dynamics Simulations. *Energy Fuels* **2009**, *23*, 1220−1229.
(27) Jian, C.; Tang, T.; Bhattacharjee, S. Molecular Dynamics Investigation on the Aggregation of Violanthrone78-Based Model Asphaltenes in Toluene. *Energy Fuels* **2014**, *28*, 3604−3613.
(28) Liu, Y.; Li, Y.; Jiang, L.; Gan, H.; Liu, H.; Li, Y.; Zhuang, J.; Lu, F.; Zhu, D. Assembly and Characterization of Novel Hydrogen-Bond-Induced Nanoscale Rods. *J. Org. Chem.* **2004**, *69*, 9049−9054.
(29) Kastler, M.; Pisula, W.; Wasserfallen, D.; Pakula, T.; Müllen, K. Influence of Alkyl Substituents on the Solution- and Surface-Organization of Hexa-*peri*-hexabenzocoronenes. *J. Am. Chem. Soc.* **2005**, *127*, 4286−4296.
(30) Bunk, O.; Nielsen, M. M.; Sølling, T. I.; van de Craats, A. M; Stutzmann, N. Induced Alignment of a Solution-Cast Discotic Hexabenzocoronene Derivative for Electronic Devices Investigated by Surface X-ray Diffraction. *J. Am. Chem. Soc.* **2003**, *125*, 2252−2258.
(31) Bai, S.; Debnath, S.; Javid, N.; Frederix, P. W.; Fleming, S.; Pappas, C.; Ulijn, R. V. Differential Self-Assembly and Tunable Emission of Aromatic Peptide Bola-Amphiphiles Containing Perylene Bisimide in Polar Solvents Including Water. *Langmuir* **2014**, *30*, 7576−7584.
(32) Su, W.; Zhang, Y.; Zhao, C.; Li, X.; Jiang, J. Self-Assembled Organic Nanostructures: Effect of Substituents on the Morphology. *ChemPhysChem* **2007**, *8*, 1857−1862.
(33) Pisula, W.; Feng, X.; Müllen, K. Tuning the Columnar Organization of Discotic Polycyclic Aromatic Hydrocarbons. *Adv. Mater.* **2010**, *22*, 3634−3649.
(34) Yoosuf Ameen, M.; Abhijith, T.; De, S.; Ray, S.; Reddy, V. Linearly Polarized Emission from PTCDI-C_8 One-Dimensional Microstructures. *Org. Electron.* **2013**, *14*, 554−559.
(35) Islam, M. R.; Sundararajan, P. Self-Assembly of a Set of Hydrophilic−Solvophobic−Hydrophobic Coil−Rod−Coil Molecules Based on Perylene Diimide. *Phys. Chem. Chem. Phys.* **2013**, *15*, 21058−21069.
(36) Jang, K.; Kinyanjui, J. M.; Hatchett, D. W.; Lee, D. Morphological Control of One-Dimensional Nanostructures of T-Shaped Asymmetric Bisphenazine. *Chem. Mater.* **2009**, *21*, 2070−2076.
(37) Buckley, J.; Hirasaki, G.; Liu, Y.; Von Drasek, S.; Wang, J.; Gill, B. Asphaltene Precipitation and Solvent Properties of Crude Oils. *Pet. Sci. Technol.* **1998**, *16*, 251−285.
(38) Mullins, O. C. The Asphaltenes. *Annu. Rev. Anal. Chem.* **2011**, *4*, 393−418.

(39) Shi, M.; Chen, Y.; Nan, Y.; Ling, J.; Zuo, L.; Qiu, W.; Wang, M.; Chen, H. $\pi-\pi$ Interaction among Violanthrone Molecules: Observation, Enhancement, and Resulting Charge Transport Properties. *J. Phys. Chem. B* **2010**, *115*, 618−623.
(40) Shi, M.; Hao, F.; Zuo, L.; Chen, Y.; Nan, Y.; Chen, H. Effect of Substituents on the Aggregate Structure and Photovoltaic Property of Violanthrone Derivatives. *Dyes Pigm.* **2012**, *95*, 377−383.
(41) Buenrostro-Gonzalez, E.; Groenzin, H.; Lira-Galeana, C.; Mullins, O. C. The Overriding Chemical Principles that Define Asphaltenes. *Energy Fuels* **2001**, *15*, 972−978.
(42) Oostenbrink, C.; Villa, A.; Mark, A. E.; Van Gunsteren, W. F. A Biomolecular Force Field Based on the Free Enthalpy of Hydration and Solvation: The GROMOS Force-Field Parameter Sets 53A5 and 53A6. *J. Comput. Chem.* **2004**, *25*, 1656−1676.
(43) Hess, B.; Kutzner, C.; van der Spoel, D.; Lindahl, E. GROMACS 4: Algorithms for Highly Efficient, Load-Balanced, and Scalable Molecular Simulation. *J. Chem. Theory Comput.* **2008**, *4*, 435−447.
(44) Van Der Spoel, D.; Lindahl, E.; Hess, B.; Groenhof, G.; Mark, A. E.; Berendsen, H. J. GROMACS: Fast, Flexible, and Free. *J. Comput. Chem.* **2005**, *26*, 1701−1718.
(45) Lindahl, E.; Hess, B.; Van Der Spoel, D. GROMACS 3.0: A Package for Molecular Simulation and Trajectory Analysis. *J. Mol. Model.* **2001**, *7*, 306−317.
(46) Berendsen, H. J.; van der Spoel, D.; van Drunen, R. GROMACS: A Message-Passing Parallel Molecular Dynamics Implementation. *Comput. Phys. Commun.* **1995**, *91*, 43−56.
(47) Riddick, J. A.; Bunger, W. B.; Sakano, T. K. *Organic Solvents: Physical Properties and Methods of Purification*; John Wiley & Sons: New York, 1986.
(48) Parrinello, M.; Rahman, A. Polymorphic Transitions in Single Crystals: A New Molecular Dynamics Method. *J. Appl. Phys.* **1981**, *52*, 7182−7190.
(49) Bussi, G.; Donadio, D.; Parrinello, M. Canonical Sampling through Velocity Rescaling. *J. Chem. Phys.* **2007**, *126*, 014101.
(50) Evans, D. J.; Morriss, O. Non-Newtonian Molecular Dynamics. *Comput. Phys. Rep.* **1984**, *1*, 297−343.
(51) Hess, B. P-LINCS: A Parallel Linear Constraint Solver for Molecular Simulation. *J. Chem. Theory Comput.* **2008**, *4*, 116−122.
(52) Essmann, U.; Perera, L.; Berkowitz, M. L.; Darden, T.; Lee, H.; Pedersen, L. G. A Smooth Particle Mesh Ewald Method. *J. Chem. Phys.* **1995**, *103*, 8577.
(53) van der Spoel, D.; Lindahl, E.; Hess, B.; van Buuren, A. R.; Apol, E.; Meulenhoff, P. J.; Tieleman, D. P.; Sijbers, A. L. T. M.; Feenstra, K. A.; van Drunen, R.; Berendsen, H. J. C. *Gromacs User Manual*, version 4.0. http://www.gromacs.org (2005).
(54) Humphrey, W.; Dalke, A.; Schulten, K. VMD: Visual Molecular Dynamics. *J. Mol. Graph.* **1996**, *14*, 33−38.
(55) Meriam, J. L.; Kraige, L. G. *Engineering Mechanics: Dynamics*, 6th ed.; John Wiley & Sons Inc.: New York, 2007.
(56) Balakrishnan, K.; Datar, A.; Oitker, R.; Chen, H.; Zuo, J.; Zang, L. Nanobelt Self-Assembly from an Organic n-Type Semiconductor: Propoxyethyl-PTCDI. *J. Am. Chem. Soc.* **2005**, *127*, 10496−10497.
(57) Balakrishnan, K.; Datar, A.; Naddo, T.; Huang, J.; Oitker, R.; Yen, M.; Zhao, J.; Zang, L. Effect of Side-Chain Substituents on Self-Assembly of Perylene Diimide Molecules: Morphology Control. *J. Am. Chem. Soc.* **2006**, *128*, 7390−7398.
(58) Israelachvili, J. N. *Intermolecular and Surface Forces*; Academic Press: San Diego, CA, 2011.
(59) Zhang, X.; Chen, Z.; Würthner, F. Morphology Control of Fluorescent Nanoaggregates by Co-Self-Assembly of Wedge-and Dumbbell-Shaped Amphiphilic Perylene Bisimides. *J. Am. Chem. Soc.* **2007**, *129*, 4886−4887.
(60) Sedghi, M.; Goual, L.; Welch, W.; Kubelka, J. Effect of Asphaltene Structure on Association and Aggregation Using Molecular Dynamics. *J. Phys. Chem. B* **2013**, *117*, 5765−5776.
(61) Frigerio, F.; Molinari, D. A Multiscale Approach to the Simulation of Asphaltenes. *Comput. Theor. Chem.* **2011**, *975*, 76−82.